CrossMark

Hierarchical Ni₃ZnN Hollow Microspheres as Stable Non-Noble Metal Electrocatalysts for Oxygen Reduction Reactions

Bo He[1,2] · Yao Yuan[3,4] · Jiacheng Wang[5] · Erum Pervaiz[4,6] · Xiangting Dong[1] · Zhigang Shao[2] · Minghui Yang[4]

Abstract

Ternary nitrides are now being considered as one of the emerging advanced functional materials owing to characteristic features and remarkable physicochemical properties that have rationale to substitute precious metals in many applied areas. The present work is focused on Ni₃ZnN hollow microspheres for the first time, synthesized by nitridation of the NiO/ZnO precursors in ammonia atmosphere. The precursors composed of 1 μm spheres were made through coordination of terephthalic acid (H₂BDC) and Zn^{2+}/Ni^{2+} cations by solvothermal treatment. The prepared bimetallic nitride is a new single crystalline ternary nitride that belongs to cubic crystal phase (space group Pm-3m, No. 221). Ni₃ZnN hollow microspheres were applied as electrocatalyst for proficiently catalyzing the oxygen reduction reactions (ORR), and exhibited very good catalytic activity with the onset potential of 0.81 V versus RHE in alkaline media. After 2000 cycles, Ni₃ZnN hollow microspheres show only a 14 mV negative shift in its half-wave potential, suggesting high stability for the ORR. Our current results can show that new ternary nitride is a potential electrocatalytic material for renewable energy resource.

Keywords MOFs · Hollow microspheres · Ternary nitrides · Solvothermal · ORR catalyst

Introduction

Designed formation of advanced functional materials using soft templates has been a focus of research in the fields of energy and environment [1]. Morphology enhanced physico-chemical aspects of a certain material can be exploited for various fields in general and catalysis in specific [2]. Nowadays, mesoporous and hollow nanostructures have attained more attention of scientific community owing to en-hanced chemical reactivity subjected to large surface area and porous nature of the materials. Depleted energy reservoirs and increasing environmental concerns have urged the material science to explore sustainable, clean and recyclable energy resources, and conversion processes. As an ideal device for energy conversion, proton exchange membrane fuel cells (PEMFCs) display superior performance over conventional devices with large energy efficiency, high power density, rel-atively low operating temperature, and less pollution [3].

Bo He and Yao Yuan contributed equally to this work.

✉ Xiangting Dong
dongxiangting888@sohu.com

✉ Zhigang Shao
zhgshao@dicp.ac.cn

✉ Minghui Yang
myang@nimte.ac.cn

1   School of Chemistry and Environmental Engineering, Changchun University of Science and Technology, Weixing road 7989, Changchun 130022, Jilin, People's Republic of China

2   Dalian National Laboratory for Clean Energy, Dalian Institute of Chemical Physics, Chinese Academy of Sciences, 457 Zhongshan road, Dalian 116023, People's Republic of China

3   University of Chinese Academy of Sciences, 19 A Yuquan Rd, Shijingshan District, 100049 Beijing, People's Republic of China

4   Ningbo Institute of Materials Technology and Engineering, Chinese Academy of Sciences, Ningbo 315201, People's Republic of China

5   State key Laboratory of High Performance Ceramics and Superfine Microstructure, Shanghai Institute of Ceramics, Chinese Academy of Sciences, 1295 Dingxi Road, Shanghai 200050, People's Republic of China

6   School of chemical and Materials Engineering (SCME), Department of Chemical Engineering, National University of Sciences and Technology (NUST), Sector H-12, Islamabad 44000, Pakistan

However, PEMFCs suffer from sluggish kinetics of oxygen reduction reactions (ORR) at the cathode side. Currently, the cathode in fuel cells mainly depends on Pt and Pt alloy catalysts, but high cost and scarcity of Pt are main barriers for its commercial applications [4]. Hence, many efforts have been paid to explore non-precious catalysts for ORR, including carbon materials [5], transition-metal oxides [6], chalcogenides [7], macrocycles [8], carbon nitrides [9], and oxynitrides [10]. Despite a lot of work has been done to explore innovative platinum-free catalysts, but none meet today's activity targets. So, there is a need to find more active catalyst to perform ORR that minimizes the operational lag of many reported materials. Therefore, dedication is intensive towards designing new catalysts with enhanced reaction effectiveness and large stability.

Transition-metal nitrides are considered as emerging electrocatalysts and an alternate to active but expensive Pt-based ORR catalysts for PEMFCs, as they possess high electrical conductivity, thermal constancy, and their electronic structures which are more close to the precious metals [11]. To date, there have been many researches about transition-metal nitrides used as catalysts for ORR, such as MoN [12], WN [13], TiN [14], Fe_2N [15], CoN [16], and CrN [17], etc. However, the research on ternary nitrides used for ORR is less reported as compared to binary nitrides. It is previously reported in the literature that the onset potential of $Co_{0.6}Mo_{1.4}N_2$ is 0.713 V (vs. RHE) in O_2 saturated 0.1 $mol \cdot L^{-1}$ $HClO_4$, which is better than $FeMoN_2$ with a response shifted by ~ 0.10 V towards more negative [18]. This stimulated us further to study ternary nitrides with designed formation and architecture morphology.

In this research work, we synthesized a new nitride Ni_3ZnN which exhibits good catalytic performance for ORR in alkaline solution. Material is critically analyzed and mechanism of electrocatalytic reaction has been studied carefully to evaluate its enhanced performance.

Experimental Details

Synthesis of Ni_3ZnN Hollow Microspheres All chemicals in the experiment were analytical grade and used without further purification. Typically, a solution of 8 mL N,N-dimethylformamide (DMF) and 5 mL of ethylene glycol is served as solvent to dissolve H_2BDC, $Ni(NO_3)_2 \cdot 6H_2O$, and $Zn(NO_3)_2 \cdot 6H_2O$ with a ratio of 1:2:1 at room temperature. After stirring for 1 h, the obtained solution was then transferred to a Teflon-lined stainless steel autoclave and maintained at 150 °C for 6 h. After cooling to room temperature, the precipitates were washed with DMF and alcohol for several times and left in a vacuum at 60 °C overnight. The obtained precursor was annealed in the muffle furnace at 500 °C for 20 min with a heating rate of 1 °C·min^{-1}, and the ashen powders were obtained. The ashen powders were nitrided in tube furnace at 600 °C for 2 h, with an ammonia flow of 150 $cm^3 \cdot min^{-1}$. Then, the sample was cooled down to the room temperature in the same flow and passivated in a flow of argon gas (20 mL·min^{-1}) for 24 h.

Characterizations

The obtained product was measured with powder X-ray Diffractometer (Rigaku Miniflex 600) using Cu-Kα radiation (λ = 1.54178 Å) in a 2θ range from 10 to 80° at 1°·min^{-1}. Thermo gravimetric analysis and differential scanning calorimetry (TG/DSC, STA-449-F3) were applied to analyze thermal behavior. The morphology and particle size of obtained product was observed through scanning electron microscopy (SEM) (JSM-7800F, Japan) and transmission electron microscopy (TEM) (FEITecnaiF20) measurement. X-ray photoelectron spectroscopy (XPS, VG ESCALAB MKII) using Mg Kα radiation was used to analyze surface valence of the materials with contaminated C as internal standard (C1s = 284.8 eV).

Electrochemical Measurement

Catalysts were performed on an MSR electrode rotator (Pine Instrument Co.) coupled with a CHI 760C workstation to evaluate ORR activities. The electrochemical cell was made up of a conventional three electrode system: a glassy carbon working electrode, an Ag|AgCl/KCl (saturated) reference electrode, and a Pt wire counter electrode. The Ni_3ZnN hollow microspheres were dissolved in a mixture of water, isopropyl alcohol, and Nafion with a ratio of 1:9:0.1 ($v/v/v$) under sonication to get 2 mg/mL ink. Afterward, 8 μL of fresh catalyst ink was dropped onto a glassy carbon (GC) disk electrode (0.196 cm^{-2}) and dried at room temperature. All the potentials reported in this work were expressed versus the reversible hydrogen electrode (RHE) based on the standard calculation method.

The cyclic voltammetry (CV) curves were obtained by cycling scan at room temperature after purging N_2 or O_2 for at least 20 min. The electrode was subjected to electrochemical treatment by potential cycling between 0.05 and 1.2 V at 100 mV·s^{-1} in 0.1 M KOH until stable voltammogram curves were obtained. For rotating disk electrode (RDE) measurements, a rotating disk electrode with a glassy carbon disk was used. The background capacitive currents were recorded in a potential range from 1.2 to 0.2 V in nitrogen-saturated electrolyte at a scan rate of 10 mV·s^{-1}. Then, linear sweep voltammograms (LSV) in oxygen-saturated electrolyte were measured at an electrode rotation speed of 1600 rpm. The oxygen reduction current was corrected by the background current.

Koutecky-Levich plots were obtained on the basis of RDE tests at different rotating rates and the electron transfer number

during ORR process can be determined from the slopes of Koutecky-Levich plots by the following equation:

$$j_{lim} = \left[0.62nFC_{O2}(D_{O2})^{2/3}v^{-1/6} \right]\omega^{1/2} \qquad (1)$$

Where j_{lim} is the limiting current density; n is the number of electrons transferred per oxygen molecule; F(96,485 C·mol^{-1}) is the Faraday constant; D_0 (1.9×10^{-5} cm^2·s^{-1}) is the diffusion coefficient of O_2 in 0.1 KOH, and C_0 (1.2×10^{-6} mol·cm^{-3}) is the concentration of O_2 in the electrolyte; v is the kinetic viscosity of the solution (0.01 cm^2·s^{-1}); and ω is the electrode rotation rate (rad·s^{-1}).

As for accelerated durability test (ADT), the electrodes were cycled between 0.6 and 1.2 V for a whole number of 2000 cycles in O_2-saturated KOH (0.1 M) with a scan rate of 100 mV·s^{-1}. Graphite counter electrode instead of Pt wire was used in the ADT to avoid the redepositing of Pt on the working electrode. Simultaneously, CV curves and ORR polarization curves were collected in aqueous KOH solution at certain cycles to record the degradation of home-made electrocatalysts and commercial Pt/C.

Results and Discussions

Under solvothermal reaction progress, the hollow microspheres of Ni-Zn metal organic framework (MOF) were designed by coordination of H$_2$BDC and Zn^{2+}/Ni^{2+} ions. These MOF hollow microspheres were transformed to NiO/ZnO

hollow microspheres by annealing the precursor microspheres in air [19]. After nitridation in ammonia, a new ternary nitride Ni$_3$ZnN was obtained. Powdered X-ray diffraction (XRD) pattern of NiO/ZnO hollow microspheres is shown in Fig. 1a. The diffraction peaks indicate that NiO and ZnO both exist in composite at the same time with different ratio. After nitridation treatment for only 1 h, there was still residual ZnO in the product as shown in Fig. 1b. Increasing the nitriding time to 2 h, ZnO can be completely converted to ternary nitride with no characteristic peaks for ZnO. It can be seen clearly that, for this Ni$_3$ZnN sample with 2 h nitridation treatment, all the diffraction peaks were indexed to cubic structure (space group Pm-3m, No. 221) without any impurity phase or unconverted precursor oxides. The calculated lattice parameter 3.766 Å was well accorded with the reported value [20, 21]. The characteristic interplanar distances d_{hkl} of (111) and (200) planes are 0.217 and 0.188 nm as calculated by the Bragg equation, respectively. In addition, the sketch map of the Ni$_3$ZnN crystal structure is displayed in the inset of Fig. 1b, which is consistent with the structures of metal intercalation compounds, such as Co$_3$ZnC, Fe$_3$ZnN, and Ni$_3$ZnC$_{0.7}$. This ensured us the synthesis of novel ternary nitride (Ni$_3$ZnN) using a facile route under mild conditions. Figure 1d shows the thermogravimetric analysis (TGA) of the prepared ternary nitride Ni$_3$ZnN to evaluate the thermal stability and behavior at various temperatures. We can observe from the TG curve that a little mass loss occurred before 436 °C, which belongs to absorbed water and other substances. When the temperature exceeded 436 °C, the weight

Fig. 1 **a** XRD pattern of NiO/ZnO hollow microspheres, **b** NiO/ZnO hollow microspheres nitrided at 600 °C for (I) 1 h and (II) 2 h (Ni$_3$ZnN hollow microspheres), **c** XRD pattern of Ni$_3$ZnN hollow microspheres annealed at 1000 °C in air, **d** differential scanning calorimetry and thermogravimetric analysis (DSC-TGA) curves of Ni$_3$ZnN
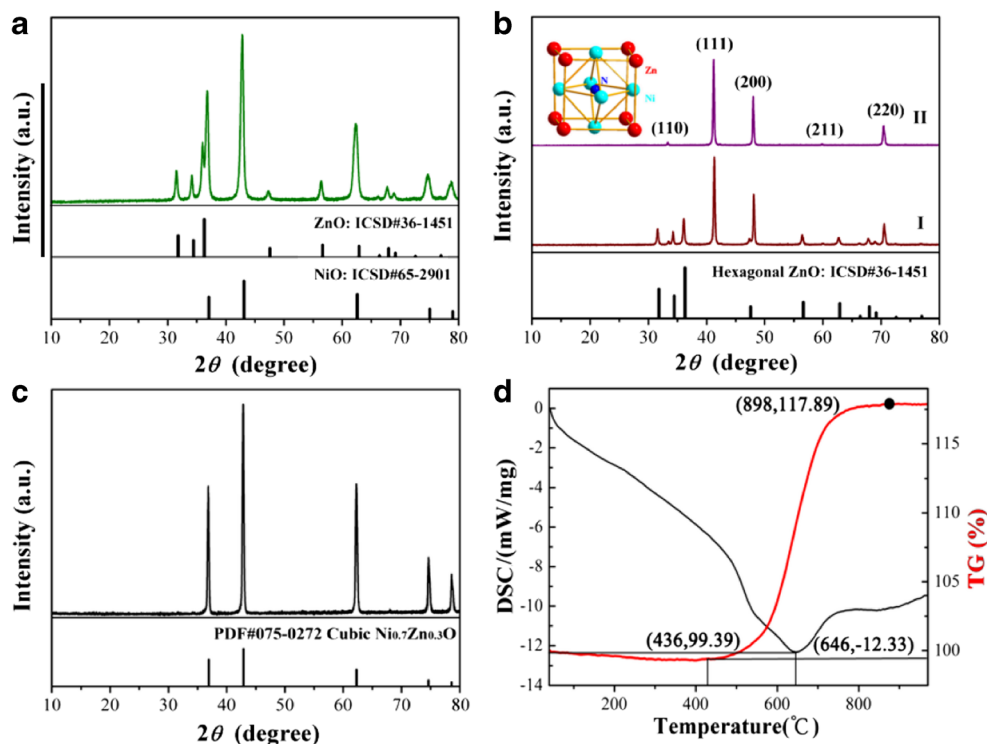
of sample began to increase, indicating the transforming progress of nitride to oxide. Further, there is an obvious exothermic peak appeared at the DSC curve, which corresponds to chemical change of nitride to oxide. The weight of the sample remained unchanged from 898 °C and the obvious weight gain is about 18.61%. Due to the stoichiometry of Ni_3ZnN, the obtained oxide should be $Ni_{0.75}Zn_{0.25}O$ that is similar to $Ni_{0.7}Zn_{0.3}O$, as shown in Fig. 1c. If all of the nitride transformed to $Ni_{0.75}Zn_{0.25}O$, the weight gain of the product would be 18.92%, which is bigger than the real weight gain. It is caused by surface partial oxidation of the nitride including 0.31 wt% oxygen.

The morphology and structure of Ni-Zn MOF precursors, NiO/ZnO, and Ni_3ZnN hollow microspheres were characterized by SEM and TEM. Figure 2a demonstrates that Ni-Zn MOF precursors are hollow and composed of regular sea urchin-like hierarchical microspheres with a size of about five microns. After annealing in air, Ni-Zn MOF precursors have turned to NiO/ZnO hollow microspheres with slightly changed urchin spherical morphology [22] as can be seen in Fig. 2b. The spherical structure is maintained but the transformation has influenced the volume of microspheres as they got shrunk with the reduced size of about 3 μm. Figure 2c, d shows the morphology of the new ternary nitride.

After the nitriding treatment, the uniform microspheres for the Ni_3ZnN still keep intact, although their sizes decreased to 1 μm. The main reason for the volume shrinkage of microspheres is the volatilization of zinc during the nitridation treatment. Moreover, the substitution of less nitrogen atoms with more oxygen sites caused a substantial decrease in the volume of hollow microspheres. Furthermore, it was evidently observed that the surface of the Ni_3ZnN hollow microspheres is not smooth and they are composed of a lot of nanoparticles with varied sizes. The as-formed hierarchical structure is much beneficial for the O_2 absorption and increased mass transfer, thus improving the catalytic activity. Figure 2e, f

Fig. 2 SEM of a Ni-Zn MOF hollow microspheres, b NiO/ZnO hollow microspheres, and c, d Ni_3ZnN hollow microspheres. e HRTEM of Ni_3ZnN hollow microspheres and f SAED pattern of Ni_3ZnN hollow microspheres
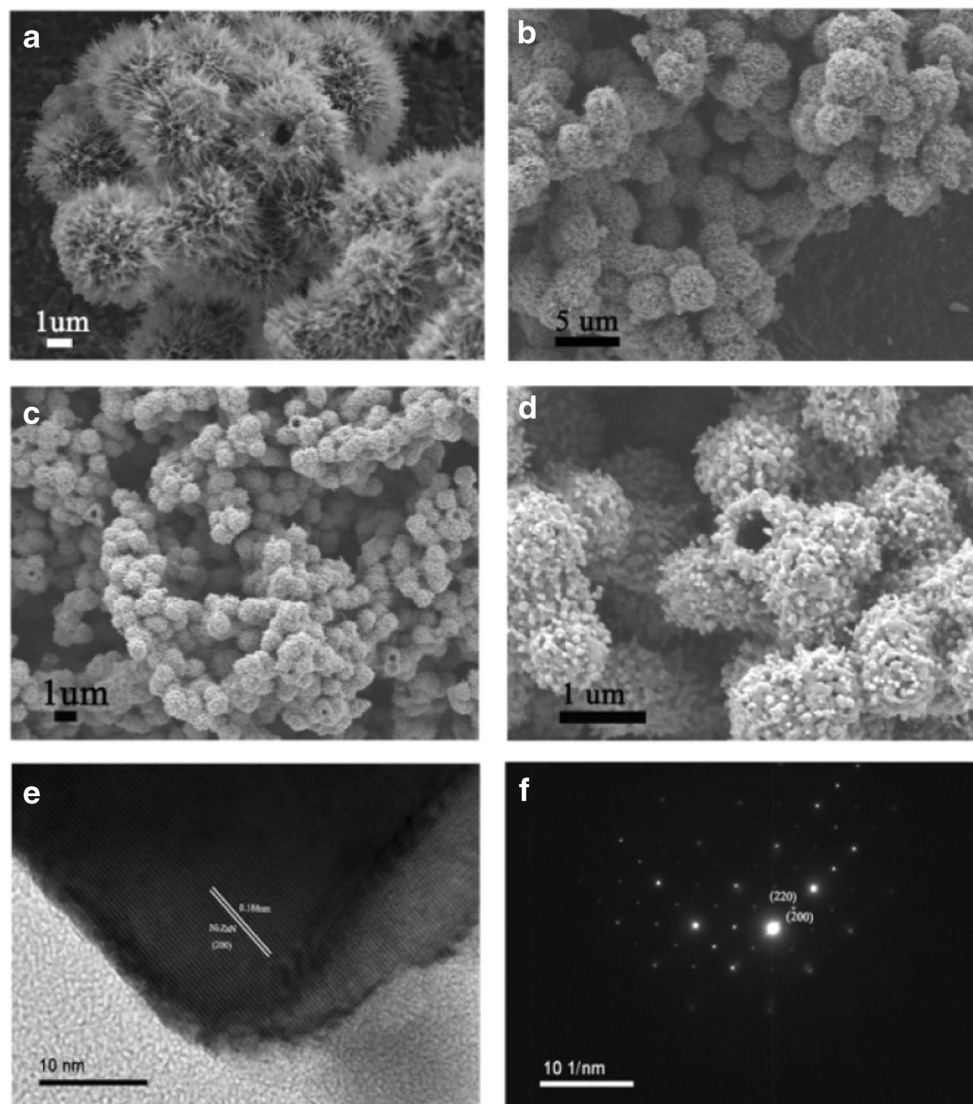
shows the HRTEM of Ni$_3$ZnN hollow microspheres and its corresponding SAED pattern, which reveal that microspheres are well crystalline. Lattice fringes of 0.188 nm can be indexed to plane (200) of cubic Ni$_3$ZnN (Fig. 2e). From the electron diffraction pattern, interplanar spaces of plane (200) and (220) are calculated to be 0.185 and 0.131 nm, respectively, which are consistent with the XRD results.

The ternary nitride was further characterized by X-ray photoelectron spectroscopy (XPS) as shown in Fig. 3. The full XPS spectrum demonstrates the ternary nitride composed of Ni, Zn, and N elements (Fig. 3a). The evident peaks in the XPS spectrum of Ni 2p for Ni$_3$ZnN at 873.16 eV (Ni 2p$_{3/2}$) and 855.49 eV (Ni 2p$_{1/2}$) belong to Ni-N while the peaks at 879.41 and 861.08 eV can be ascribed to Ni oxide species, which further suggest that facial oxidation exists in Ni$_3$ZnN [23]. Moreover, with comparison to the XPS spectrum of Ni 2p for Ni$_3$N, a negative shift occurred in Ni-N for Ni$_3$ZnN (Fig. 3b). The two main peaks in Zn 2p XPS spectrum (Fig. 3c) are assigned to Zn-N [24]. The N 1s spectra of Ni$_3$ZnN and Ni$_3$N can be fitted into three peaks (Fig. 3d). The peaks located at 397.74 and 397.43 eV belong to N-Ni bond [25], and the other peaks in the N 1s spectra at the positions of 399.54, 398.53, 399.59, and 398.72 eV are ascribed to N-Zn bond and NH$_3$ or amines like N [26]. Also, there is a negative shift occurring in Ni$_3$ZnN.

Cyclic voltammetry (CV) was applied to evaluate the electrocatalytic activity of the prepared hierarchical Ni$_3$ZnN hollow microspheres for ORR in a 0.1 M KOH saturated with N$_2$

or O$_2$ as shown in Fig. 4a. It can be observed that CV of Ni$_3$ZnN electrode presents an obvious redox peak at around 0.65 V in O$_2$-saturated 0.1 M KOH which can be recognized as reduction peak of oxygen on Ni$_3$ZnN microspheres while CV of Ni$_3$ZnN electrode in N$_2$-saturated 0.1 M KOH demonstrates no obvious reduction peak. This comparison implies that the ORR proceeds on the surface of the Ni$_3$ZnN electrode. Figure 4b shows the linear scan polarization curves for ORR performance of ternary nitride (Ni$_3$ZnN) in O$_2$-saturated 0.1 M KOH with a scan rate of 10 mV·s^{-1} at 1600 rpm. It can be found that the onset potential of Ni$_3$ZnN for ORR is 0.81 V (vs. RHE) much lower than 0.98 V (vs. RHE), characteristic onset potential of commercial Pt/C [27]. Although onset potential of Ni$_3$N and Ni$_3$ZnN is similar, the limiting diffusion current of hollow microspherical Ni$_3$ZnN (− 3.48 mA·cm^{-2}) is larger than Ni$_3$N (− 2.97 mA·cm^{-2}), as shown in Fig. 4b. A higher current density of hollow microspherical Ni$_3$ZnN indicates a more active performance than Ni$_3$N. As a result, the performance distinction between Ni$_3$ZnN and Ni$_3$N could be attributed to their disparate electronic structures, and the introduction of zinc can reduce the charge transfer resistance between catalyst and electrolyte. In addition, the active sites were closely related to zinc, thus to further improve its ORR catalytic activity. The mass activities of commercial Pt/C, Ni$_3$ZnN, and Ni$_3$N are calculated as shown in Fig. 4c. We have found that the mass activity of Ni$_3$ZnN is 42.6 A·g^{-1}, which is lower than that of Pt/C, but higher than that of Ni$_3$N, corresponding to the other results.

Fig. 3 **a** XPS spectra of Ni$_3$N and Ni$_3$ZnN, and high-resolution XPS spectra of **b** Ni 2p, **c** Zn 2p, **d** N 1s

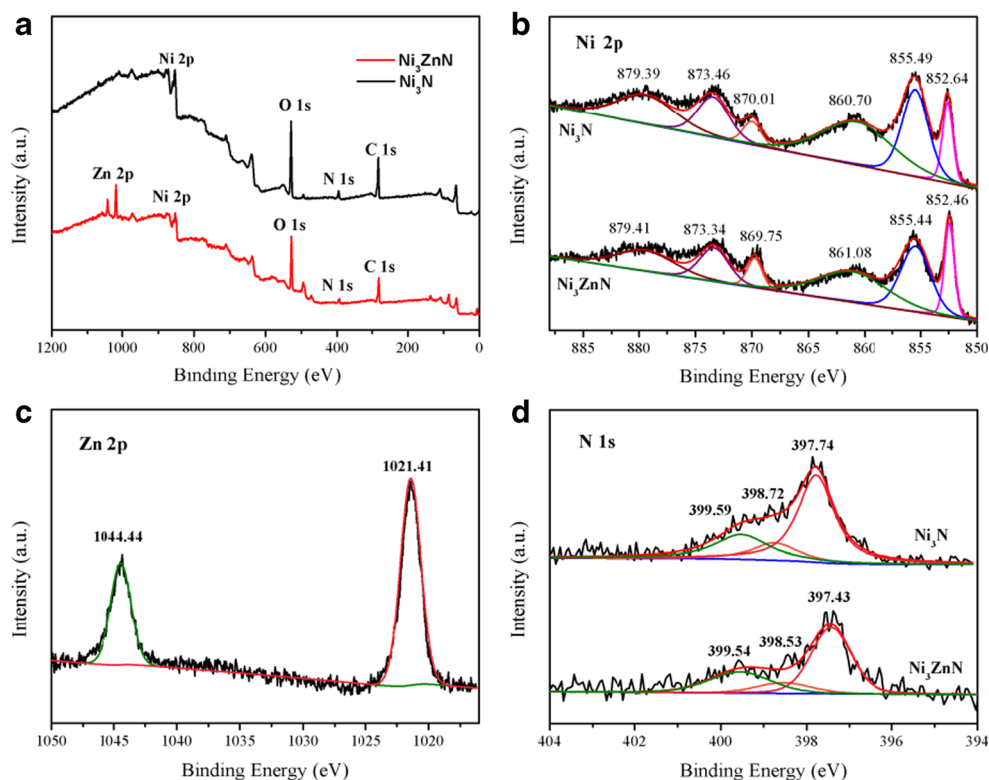**Fig. 4** **a** CV curves of Ni₃ZnN at a scan rate of 50 mV·s⁻¹ in O₂-saturated 0.1 M KOH solutions, **b** RDE polarization curves of Ni₃ZnN, Ni₃N and 20% Pt/C, **c** mass activities of Ni₃ZnN, Ni₃N and 20% Pt/C at the maximum limiting diffusion current, **d** RDE polarization curves of Ni₃ZnN in O₂-saturated 0.1 M KOH with various rotation rates at a scan rate of 10 mV·s⁻¹, **e** Koutecky-Levich plots of Ni₃ZnN at different potentials, and **f** the RDE polarization curves of Ni₃ZnN before and after 2000 CV cycles (rotating speed and the scan rate were 1600 rpm and 10 mV·s⁻¹, respectively)
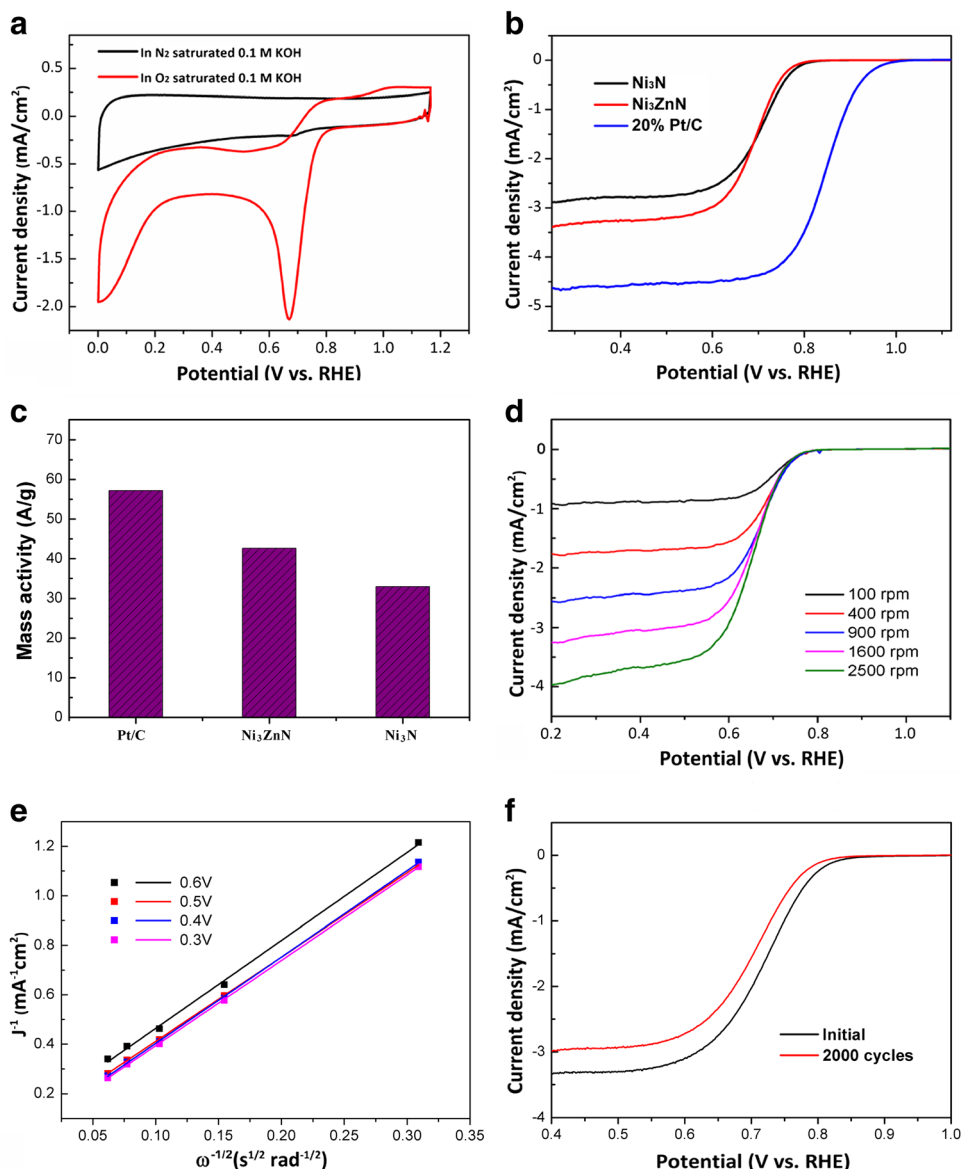
With an increasing scan rate, the limiting diffusion current of Ni₃ZnN is enhanced (Fig. 4d). Besides, we have further obtained Koutecky-Levich plots of Ni₃ZnN which results from linear sweep voltammogram (LSV) curves at different rotation speeds (Fig. 4e). Using the formula and slopes of Koutecky-Levich plots, the average electron-transfer number (n) is calculated to be 2.49 in the range of 0.3 to 0.6 V, implying the ORR reaction on the Ni₃ZnN is two-electron dominant pathway. After 2000 cycles, Ni₃ZnN hollow microspheres show only a 14 mV negative shift in its half-wave potential (Fig. 4f). Also, the limiting diffusion current of Ni₃ZnN at 0.4 V was sustained at 89.4% with comparison to initial cycle. This demonstrates good stability of the electrocatalyst in alkaline media that can be a result of hollow microsphere nature providing suitable interface for ORR. Successful introduction of zinc certainly has improved the efficiency of ORR, although not as good as we previewed. As described in the XPS results,

lower binding energy of Ni-N in Ni₃ZnN relates much higher electron density for the transfer of electrons to oxygen in co-operation of Zn(0), while the Ni in Ni₃N possesses higher binding energy leading to lower efficiency for ORR. So both factors, hollow structure of Ni₃ZnN and low binding energy of Ni in cooperation of Zn(0), lead to a greater limiting diffusion current for ORR.

Conclusions

In summary, a new ternary nitride of hollow spherical structure with a size of 1 μm has been synthesized by the combination of solvothermal, calcination, and nitridation. From XRD, SEM, and HRTEM results, the as-prepared Ni₃ZnN hollow microspheres are composed of nanosized particles with a single crystalline structure of cubic phase (space group

Pm-3m, No. 221). As an electrocatalyst for ORR, the onset potential of Ni_3ZnN hollow microspheres is 0.81 V (vs. RHE) in alkaline media. In spite of the similar onset potentials of Ni_3ZnN and Ni_3N, the superior limiting diffusion current is obtained for Ni_3ZnN hollow microspheres. Moreover, the ORR performance of Ni_3ZnN hollow microspheres kept stable in alkaline solution, for which the half-wave potential has a negative shift of only 14 mV, after 2000 cycles' CV scan.

References

1. L. Han, S. Dong, E. Wang, Adv. Mater. **28**, 9266–9291 (2016)
2. S. Wang, X. Wang, Small **11**, 3097–3112 (2015)
3. X. Ge, A. Sumboja, D. Wuu, T. An, B. Li, F.W.T. Goh, et al., ACS Catal. **5**, 4643–4667 (2015)
4. Y. Nie, L. Li, Z. Wei, Chem. Soc. Rev. **44**, 2168–2201 (2015)
5. Z.-J. Jiang, Z. Jiang, J. Mater. Chem. A **2**, 14071–14081 (2014)
6. J. Wang, H.L. Xin, J. Zhu, S. Liu, Z. Wu, D. Wang, J. Mater. Chem. A **3**, 1601–1608 (2015)
7. W. Zeng, L. Wang, H. Shi, G. Zhang, K. Zhang, H. Zhang, et al., J. Mater. Chem. A **4**, 8233–8241 (2016)
8. H.L. Rongrong Chen, D. Chu, G. Wang, J. Phys. Chem. C **113**, 20689–20697 (2009)
9. H. Yang, J. Liu, J. Wang, C.K. Poh, W. Zhou, J. Lin, et al., Electrochim. Acta **216**, 246–252 (2016)
10. C. Pozo-Gonzalo, O. Kartachova, A.A.J. Torriero, P.C. Howlett, A.M. Glushenkov, D.M. Fabijanic, et al., Electrochim. Acta **103**, 151–160 (2013)
11. D.H. Zhongwei Chen, A. Yu, L. Zhang, J. Zhang, Energy Environ. Sci. **4**, 3167–3192 (2011)
12. B. Cao, J.C. Neuefeind, R.R. Adzic, Inorg. Chem. **54**, 2128–2136 (2015)
13. H. Yan, C. Tian, L. Wang, et al., Angew. Chem. Int. Ed. **54**, 6325–6329 (2015)
14. Y. Wang, R. Ohnishi, E. Yoo, et al., J. Mater. Chem. **22**, 15549–15555 (2012)
15. L. Liu, X. Yang, N. Ma, Small **12**, 1295–1301 (2016)
16. L. An, W. Huang, N. Zhang, J. Mater. Chem. A **2**, 62–65 (2014)
17. L. Zhao, L. Wang, P. Yu, Chem. Commun. **51**, 12399–12402 (2015)
18. B. Cao, J.C. Neuefeind, R.R. Adzic, P.G. Khalifah, Inorg. Chem. **54**, 2128–2136 (2015)
19. G.C. Li, P.F. Liu, R. Liu, M. Liu, K. Tao, S.R. Zhu, et al., Dalton Trans. **45**, 13311–13316 (2016)
20. M. Uehara, A. Uehara, K. Kozawa, T. Yamazaki, Y. Kimishima, C. Physica, Superconductivity **470**, S688–S690 (2010)
21. C. Li, W.G. Chen, F. Wang, S.F. Li, Q. Sun, S. Wang, et al., J. Appl. Phys. **105**, 123921–123930 (2009)
22. J. Fang, Y.F. Yuan, L.K. Wang, H.L. Ni, H.L. Zhu, J.S. Gui, et al., Mater. Lett. **111**, 1–4 (2013)
23. Y. Wang, C. Xie, D. Liu, X. Huang, J. Huo, S. Wang, ACS Appl. Mater. Interfaces **8**, 18652–18657 (2016)
24. P.S. Ying Xiao, M. Cao, ACS Nano **8**, 7846–7857 (2014)
25. Y. Yu, W. Gao, Z. Shen, Q. Zheng, H. Wu, X. Wang, et al., J. Mater. Chem. A **3**, 16633–16641 (2015)
26. M. Mapa, C.S. Gopinath, Chem. Mater. **21**, 351–359 (2009)
27. J. Li, Q. Wang, K. Liu, J. Jiang, D. Qian, J. Li, et al., Mater. Lett. **186**, 189–192 (2017)